Journal of Materials Chemistry C

Accepted Manuscript

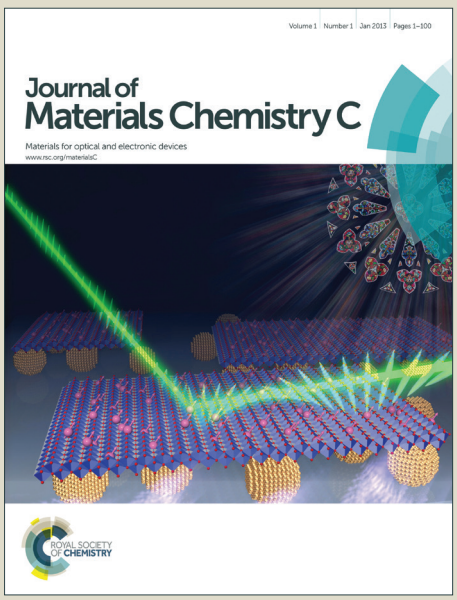

ROYAL SOCIETY OF CHEMISTRY

www.rsc.org/materialsC

Journal Name

RSCPublishing

ARTICLE

TiO_2-anthraquinone hybrids: From quantum-chemical design to functional materials

Cite this: DOI: 10.1039/x0xx00000x

J. Mech, [a] K. Mech[b] and K. Szaciłowski[a,b],*

Received 00th January 2012,
Accepted 00th January 2012

DOI: 10.1039/x0xx00000x

www.rsc.org/

A series of materials based on titanium dioxide nanoparticles and anthraquinone dyes have been modelled using quantum mechanical minimalistic model. On the basis of the computational results some spectral and photoelectrochemical properties of these materials have been predicted. Experimental studied indicate that the quantum-chemical predictions are correct. New materials exhibit interesting switching properties and moderate photosensitization towards visible light. Furthermore, on the basis of excited state properties of dye-semiconductor hybrids diverse photocatalytic properties, including activation of molecular oxygen, can be predicted.

Introduction

Photoelectrochemical photocurrent switching (PEPS) effect was reported for the first time in 2006,[1] but some preliminary reports on photocurrent switching in nanoparticulate wide band gap semiconductors (mostly TiO_2) were described earlier.[2-4] Most of these materials reported to date are based, with some exceptions,[5-9] on titanium dioxide.[1, 10-22] Its surface is usually modified with inorganic, organometallic or organic species with desired optical and electrochemical reactivity. First of all the modifier itself should absorb visible light or be engaged in chromogenic interaction with titanium(IV) ions. Furthermore, it should undergo reversible redox processes within narrow electrochemical window. These conditions sine qua non do not guarantee the occurrence of the PEPS effect. Appropriate yields of interfacial electron transfer, specific adsorption of sacrificial electron acceptor and/or catalytic properties of the surface towards reduction of molecular (dissolved) oxygen are also of crucial importance.[23] Materials which can be regarded as two coupled photocurrent generators also show this effect, but on a very different basis.[19, 24, 25] The PEPS effect itself constitutes an universal platform for construction of various optoelectronic devices, including logic gates, demultiplexers, computing circuits, reconfigurable devices and sensors.[23, 26-28] Despite high utility of PEPS materials they were usually prepared by trial-and-error approach via combinations of numerous nanoparticulate wide band gap semiconductors with appropriate organic molecules or transition metal complexes. Resulting materials show photocurrent switching properties based on various phenomena, which usually are not possible to predict at the material design stage. Therefore, in order to facilitate the design of novel hybrid materials for PEPS effect-based optoelectronic devices the quantum-chemistry-based approach is suggested.

Four different species, belonging to the family of anthraquinone derivatives: alizarin (**1**), quinizarin (**2**), anthrarufin (**3**) and chrysazin (**4**) were used as model compounds for quantum-chemical investigation and subsequently used to modify the TiO_2 nanoparticles. All these compounds are stable and easily available from both synthetic and natural sources, therefore they are compatible with the concept of green chemistry, however application of organic solvents during the synthesis of dye-semiconductor hybrids cannot be avoided. Alizarin itself is a well-known photosensitizer of TiO_2[16, 29-39] and a preliminary report on anthrarufin can be also found.[17] **1** is a molecule composed of the central quinone ring, the catechol ring on the one side and the benzene ring on the opposite side. Similar structure can be found in alizarin isomers (**2**, **3**, **4**). The only difference between them is location of one of the hydroxyl groups. It was already found that despite apparent structural similarities these compounds differ in spectral properties, redox potentials and intermolecular supramolecular interactions.[40] Therefore it is hypothesized that the geometrical diversity of four anthraquinone derivatives will be also reflected in different photoelectrochemical properties of hybrid materials based on TiO_2. This work presents how simple quantum-chemical models can be used to predict properties and photoreactivity of hybrid inorganic-organic materials.

Experimental

Materials and methods

Organic compounds used in synthesis were delivered by Acros (**1**) and Alfa Aesar (**2**, **3** and **4**). All these compounds of highest purity available were used as purchased. HPLC grade solvents, acetonitrile (ACN) and dimethylformamide (DMF) were supplied by POCH and Sigma Aldrich, respectively. TiO_2 (Evonic P25) is a mixture of anatase (80%) and rutile (20%). Diffuse reflectance spectra of pure components as well as of hybrid materials were recorded on Lambda 950 spectrophotometer (Perkin Elmer, USA) equipped with 150 mm integration sphere. For reflectance spectroscopy the samples

were dispersed in spectrally pure $BaSO_4$ (Sigma Aldrich). The same $BaSO_4$ was used as a white standard. Recorded reflectance values were converted to the Kubelka-Munk function (α'_{KM}) according to Eq. 1:

$$\alpha'_{KM}(h\nu) = \frac{\left[1 - R(h\nu)\right]^2}{2R(h\nu)} \quad (1)$$

where: *R* stands for reflectance. Thus obtained spectra were normalized by multiplication of α'_{KM} by the energy of the light quantum (*hν*) in order to preserve the Gaussian envelope of electronic transitions:[41]

$$\alpha_{KM}(h\nu) = \alpha'_{KM}(h\nu) \cdot h\nu \quad (2)$$

Photoelectrochemical characterization was performed using a photoelectric spectrometer (Instytut Fotonowy, Poland) composed of stabilized 150 W xenon arc lamp and computer-controlled monochromator coupled with the SP-300 potentiostat (Bio_logic, France). Experiments were carried out in aqueous KNO_3 solutions (0.1 M) equilibrated with air or purged with argon and stored under argon blanket. Working electrodes of ca. 1 cm^2 surface area were prepared from ITO-covered polyethyleneterephthalate (PET) foil. A drop of aqueous suspension of the studied material was cast onto the ITO surface and dried in a stream of hot air. Such films were stable enough for at least two independent measurements. Surface photovoltage spectra were measured using the Kelvin probe detection system (Besocke Delta Phi, Germany) coupled with photoelectric spectrometer via liquid lightguide (Lumatec, Germany). Samples dispersed on ITO foil were illuminated through oscillating grid electrode and surface photovoltage was recorded as a function of incident light wavelength.
Differential pulse voltammetry (DPV) measurements were conducted in a three electrode configuration. The platinum disc working electrode (1 mm diameter), Pt coil (0.24 mm in diameter, 10 cm long) and Ag/AgCl (sat. KCl) reference electrode were used throughout. All experiments were performed in DMF solution using 0.1 M tetrabutylammonium tetrafluoroborate ($TBABF_4$) as a supporting electrolyte, whereas the concentration of the studied compounds were ca. 1 mM. In the case of hybrid materials a drop of aqueous suspension was cast onto a Pt disc and dried with a stream of hot air. All potentials are given vs. standard hydrogen electrode (SHE). Ferrocene in DMF was used to calibrate the reference electrode using the standard potential of ferrocene/ferrocenium couple equal to 0.7 V.[42] Before experiment the electrolyte was purged with nitrogen for at least half an hour and during measurement a nitrogen blanket was used to prevent contamination of the sample.

Modified titanium dioxide was prepared as follows. Small amount of chromophore (25 mg) was dissolved in 5 ml ACN (**1**, **2** and **4**) or DMF (**3**). The solution was added to 150 mg of TiO_2. The suspension was sonicated in ultrasonic bath (5 min) in order to provide better adsorption of molecules on the surface of TiO_2. To remove unadsorbed dyes materials was washed 5 times with the same solvent. In the case of DMF the product was further washed with isopropanol or water in order to remove non-volatile solvent.

Computational details

The geometry optimization in the ground state was performed by the density functional theory (DFT) using the B3PW91 hybrid functional (Becke three parameter Perdew-Wang 1991)[43-45] and the 6-311+G(d,p) basis set. This choice is motivated by better performance (as compared with B3LYP) in the case of transition metal complexes, especially used as models mimicking the modified semiconducting surfaces. In contrast to commonly used B3LYP, the B3PW91 functional uses only the nonlocal correlation energy of the PW91, while the local correlation energy comes from the Vosko-Wilk-Nussair functional. Therefore it is more suited for the uniform electron gas limit.[46] Importantly, the B3PW91 functional yield very reliable data for anthraquinone dyes.[40] Model used in calculations consist of deprotonated chromophore molecules bounded to the $Ti(OH)_2^{2+}$ ion (Figure 1). This model, taken from literature,[39, 47] despite its simplicity, reproduces well the absorption spectra and electronic structure of hybrid material. UV-Vis spectra were calculated using the time dependent density functional theory (TD-DFT) at the same level of theory. The vertical excitation energy was calculated for the first 20 singlet states in the ground state geometry. All computation investigations were performed by Gaussian09 Rev. A.02. Structures of test complexes were chosen on the basis of preliminary computational experiments on dye molecules [40] and experimental data.[17] It was assumed that all dyes bind in bidentate fashion with concomitant deprotonation (Figure 1).[35]

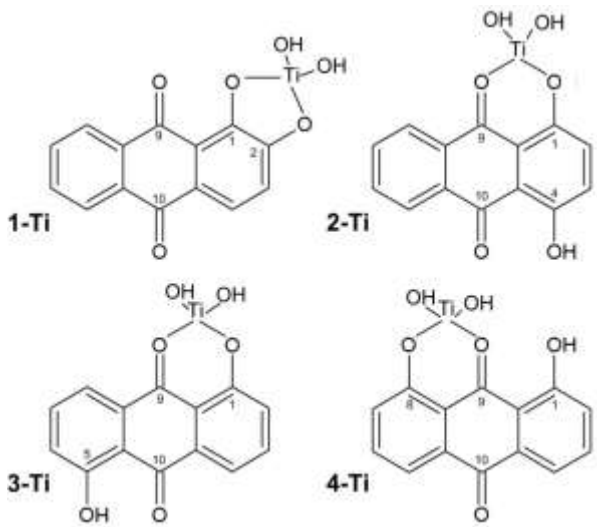

Figure 1. Structures of model dye-titanium(IV) complexes.

Results and discussion

Effective modifier of TiO_2 should be characterized by strong absorption of visible light and the presence of binding groups to the

TiO_2 surface. The previous criteria is mostly preserved in the case of $\pi \rightarrow \pi^*$ or $n \rightarrow \pi^*$ transition, characteristic for aromatic structures. The latter criterion is realized by the presence of hydroxyl and carbonyl functional groups. The following condition is a chemical stability. Anthraquinone derivatives are chemically stable and take part in quasi reversible chemical reaction. Anthraquinone derivatives usually are decent TiO_2 photosensitizers[39, 48-50] but it is not enough to exhibit the PEPS effect. In the PEPS effect two types of photocurrent switching can be distinguished: by changing of applied external potential or by changing wavelength of incident light. In most cases both types of photocurrent switching are visible. The character of photocurrent switching potential as a function of applied external potential and wavelength of incident light results from interplay between electron transfer thermodynamics and kinetics. The former criterion provides appropriate arrangement of energy levels, whereas the latter deals with competitive reaction pathways. The thermodynamic criteria can be clearly evaluated using theoretical approach. Some preferences towards different reaction pathways can be deduced theoretically, however with a lower confidence. It the following sections we present computational results on TiO_2 modified with four anthraquinone dyes and compare this data with experiments.

All studied molecular systems are almost planar molecules with titanium(IV) center only slightly protruding out of the plane of the aromatic system. Dihedral angles measured for fully optimized geometries amount 8.94, 1.40, 0.06 and 2.74 degrees for **1-Ti**, **2-Ti**, **3-Ti** and **4-Ti**, respectively. In all the cases two hydroxyl ligands at titanium ion are located on both sides of aromatic plane and deviated from the normal to the place by ca. 22 degrees, which corresponds to slightly deformed tetrahedral coordination of titanium.

The strength of interaction between titanium(IV) centers and organic dyes can be evaluated on the basis of titanium-oxygen bond lengths. These bonds are the shortest in the case of **1-Ti**: 1.348 Å for a bond to oxygen in the position 1 and 1.351 Å for a bond to oxygen in the position 2. In **2-Ti** these bonds are much longer: 1.833 and 1.895 Å. The shorter one involves phenolic oxygen, while the longer the carbonyl one. **3-Ti** presents the same arrangement with respective bond lengths of 1.824 and 1.903 Å. The largest discrepancy in bond lengths between phenolic and carbonyl oxygen atoms can be observed in the case of **4-Ti**: 1.807 vs. 1.925 Å.

Dye **1** shows its distinctness also in Mullikan charge population analysis. In all the cases the titanium ion within the test structure bears significant positive charge, however in the case of **1-Ti** this charge is the lowest (0.971). Other compounds exhibit significantly higher charges of 1.280, 1.282 and 1.329 for **2-Ti**, **3-Ti** and **4-Ti**, respectively. Slightly lower charge in the case of **1-Ti** is easily explained by lower overall charge of the test molecule (0, vs +1 in other cases). Charge distribution is presented in the form of colour-coded electrostatic potential maps which allow more direct comparison of surface charge distribution irregularities of test molecules (Figure 2). It can be noticed that the quinone moiety serves in all studied systems as a local (intramolecular) electron acceptor, while the terminal rings are electron donors. Similar charge distribution (negative quinone moiety and positive side rings) can be observed in the case of dye molecules themselves, which is related to strong electron withdrawing effect of quinonic carbonyls.[51] Directional charge location results in the formation of a significant dipole moment, which is 3.44 D for **1-Ti**, 6.82 D for **2-Ti**, 6.83 D for **3-Ti** and 5.40 for **4-Ti**. The Mulliken charge distribution, in general, does not reveal any significant differences between studied systems in the ground state, however the **1-Ti** system shows the strongest intramolecular donor-acceptor character within the organic moiety. Negative charge is located at oxygen atoms and carbon atoms of the side rings, whereas positive charge is located at the titanium atom and carbon atoms within carbonyl bridges. The frontier orbital analysis indicates that in all studied cases the aromatic system is an electron donor, whereas the titanium center is an electron acceptor (Figure 3). In the latter case, however, the LUMO orbitals are also partially delocalized over the ring system. It may indicate a competitive character of interaction between titanium(IV) centers and anthraquinone dyes in terms of electron donor-acceptor interactions.

The main transition for all modeled structures is the HOMO→LUMO transition with insignificant contribution of higher excitations. This observation is confirmed by Prezhdo *et al.*.[52] In detailed description the first singlet excited state **1-Ti** consist of HOMO→LUMO and HOMO→LUMO(+1) excitations which dominating HOMO→LUMO one. Both are charge transfer transitions, with LUMO localized mainly at the titanium atom and LUMO(+1) localized mainly at anthraquinone rings (Figure 3). The second singlet transition of **1-Ti** has negligibly low oscillator strength. Subsequent relevant singlet transition (the third transition), is purely HOMO-LUMO(+2). This transition is characterized by the pure charge transfer from the side ring to the titanium centre. For **2-Ti** two transitions with relevant oscillator strength: the first singlet transition (oscillator strength 0.0758) and the fourth singlet transition (oscillator strength 0.0204). In the first transition HOMO→LUMO and HOMO→LUMO(+2) excitations are involved, whereas in the fourth transition HOMO(−1)→LUMO, HOMO(−2)→LUMO and HOMO→LUMO(+2) are involved. **3-Ti** has two significant transitions, similarly to **1-Ti**: the first and the third singlet transitions. The first transition includes HOMO→LUMO and HOMO(−2)→LUMO. The third transition consist only from HOMO(−1)→LUMO. The last model, **4-Ti** has HOMO→LUMO as the dominant transition in the second singlet state and two less significant ones: HOMO(−2)→LUMO and HOMO(−1)→LUMO. In the third singlet transition significant are HOMO(−1)→LUMO and HOMO→LUMO excitations.

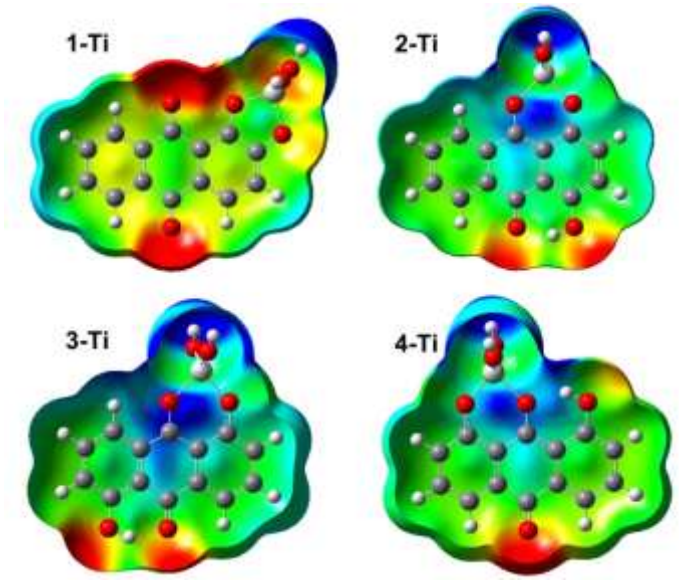

Figure 2. Electrostatic potential mapped onto the total electron density in the ground state of the studied anthraquinone derivatives. Calculations were made using DFT technique at the B3PW91/6-311 + G(d,p) level of theory. Areas marked in red and yellow are rich in electric charge, while cyan and blue are depleted in electric charge. Green color depicts neutral regions.

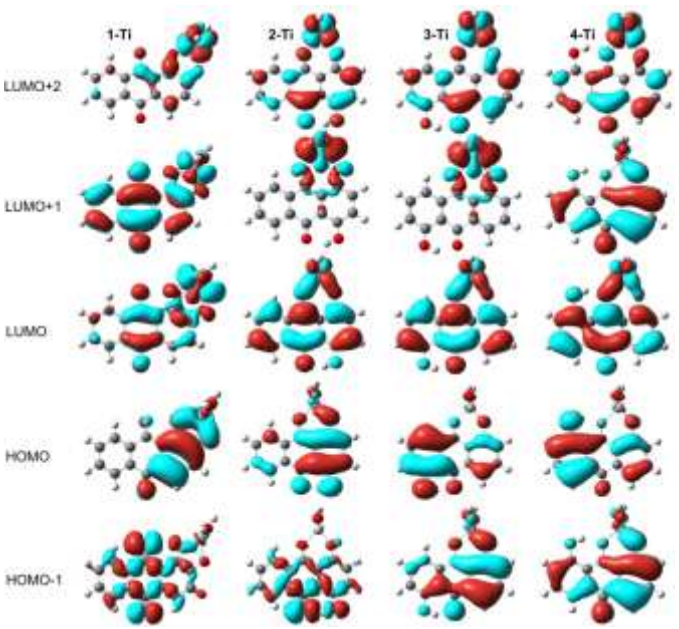

Figure 3. Contours of the frontier molecular orbitals of studied anthraquinone derivatives adsorbed at TiO_2. Calculation were carried out using DFT technique at the B3PW91/6-311 + G(d,p) level of theory.

Excited state of hybrid materials

TD-DFT technique was used for calculations of electronic structure of the excited states. Results are presented as electrostatic differential potential diagrams in Figure 4. **1-Ti** upon excitation reveals change in the surfaces charge, in a way increasing its donor properties. Negative charge is mainly located at carbonyl moiety opposite to the titanium ion binding site. Such a spatial charge reorganization may indicate the tendency of this system to serve as an excited-state electron donor. This in turn may results in significant reduction of sacrificial electron acceptor and cathodic photocurrent generation. In the case of **2-Ti** negative charge is divided into two peripheral rings, while the central ring gathers positive charge. This charge distribution, with zero dipole momentum in the excited state, does not promote any of photocurrent directions, neither cathodic, nor anodic. The **3-Ti** and **4-Ti** models exhibits significant charge transfer towards titanium center rendering the quinone ring system even stronger electron acceptor as compared to the ground state. Such nature of the lowest excited state should in principle result in an increased efficiency of electron injection to the conduction band of titanium dioxide.

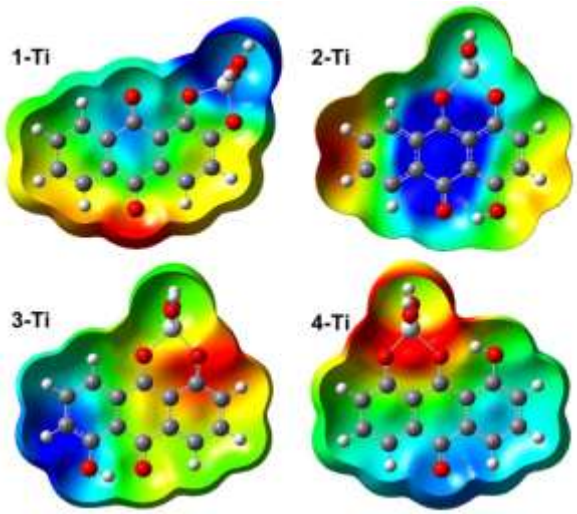

Figure 4. Differential electrostatic potential mapped onto the electron density isosurface of the studied compounds, using TD-DFT technique, at the B3PW91/6-311 +G(d,p) level of theory. Areas marked in red and yellow bear negative electric charge, while cyan and blue are depleted of electron density, upon excitation. Green color depicts regions with no net charge density change.

Electronic spectra

The interaction between dye molecules and TiO_2 is manifested by a bathochromic shift of the absorption spectra of the chromophore (Figure 5). Absorption edge of TiO_2 (ca. 3.2 eV) is located at energies much higher than absorption maximum of studied molecules (ca. 2.5 eV) and it is not disturbed by organic-inorganic interaction. Single components and hybrid materials spectra were measured in the solid state and compared (Figure 5). Analyzing the spectra we conclude that spectrum of each chromophore is shifted to lower energy and the spectral envelopes are well-preserved after absorption at TiO_2. The latter does not exclude the fact that spectra of hybrid materials have more regular shapes, what can be explained by elimination of tautomeric forms during the synthesis. Tautomers possess hydroxyl and carbonyl groups located in different positions, which usually is not privileged during the formation of chemical bond with TiO_2 .[51]

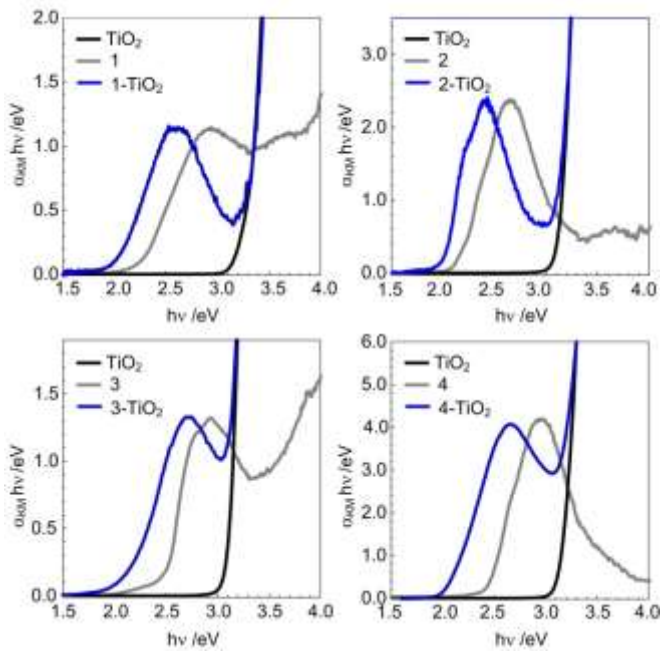

Figure 5. Absorption spectra of pure compounds and hybrid materials. Gray, black and blue lines indicate: pure chromophore, TiO_2 and hybrid material respectively.

Values of the bathochromic shift, collated in Table 1, are different for particular dihydroxyanthraquinone isomers.

Table 1. Energies of absorption band maxima of free and titania-bound dyes and the value of the bathochromic shift (in eV).

compound	pure dye	Dye-TiO_2	ΔE
1	2.89	2.53	0.33
2	2.66	2.41	0.25
3	2.96	2.73	0.23
4	2.93	2.66	0.27

The largest shift (0.33 eV) is observed for **1-TiO_2** and the lowest (0.23 eV) for **3-TiO_2**. These values nicely reflects the bonding modes of studied dyes. Interaction via two hydroxyl groups (**1** and to some extent **4**) results in shifts significantly higher that the interaction via one hydroxyl only.

Flat-band potential

Flat band potential (E_{fb}) is the main parameter determining the electrochemical and catalytic properties of semiconducting materials. The Mott-Schottky measurements yield the value of for pure TiO_2 of −0.25 V vs standard hydrogen electrode (SHE). Modification of TiO_2 by anthraquinone dyes influences this value more or less, dependently of type of interactions taking place at molecules interface (Table 2). It seems that only alizarin significantly shifts the flat band potential to more cathodic values, while the change recorded for other dyes is insignificant. Therefore it can be concluded that only alizarin binds the surface as dianion, while other dyes do in monoanionic form, as the shift in flat band potential can be directly related to the electric charge at the surface.

Table 2. Flat band potential values for pure and modified TiO_2.

Name	TiO_2	**1-TiO_2**	**2-TiO_2**	**3-TiO_2**	**4-TiO_2**
E_{fb} vs SHE /V	-0.25	-0.41	-0.27	-0.26	-0.26

Redox states of hybrid materials

One of the important electrochemical parameter characterizing hybrid materials is redox potential. Redox potentials values of investigated hybrid materials were determined by use of differential pulse voltammetry technique (DPV) (Figure **6**).

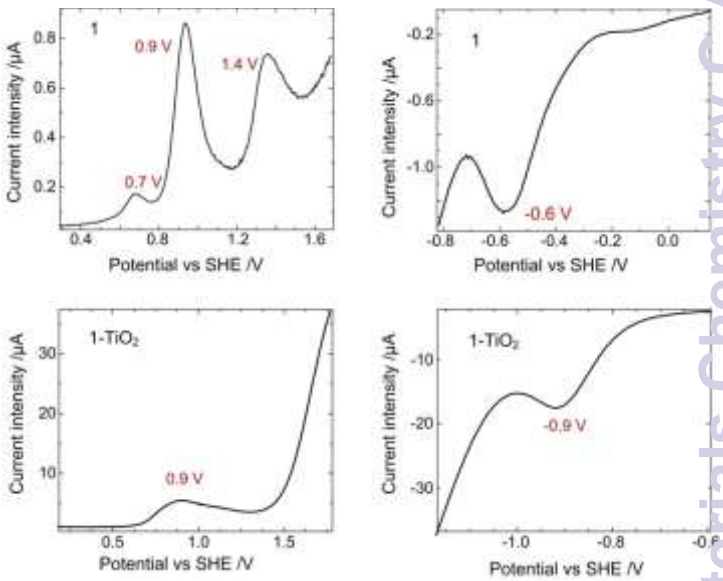

Figure 6. Differential pulse voltammograms of **1** and **1-TiO_2** in DMF solution in a presence of $TBABF_4$.

Table 3. Values of redox potentials for pure chromophores and the same adsorbed at TiO_2.

Sample	E_{ox} /V vs SHE	E_{red} /V vs SHE	E_{ox}-E_{red} /V	ΔE_{ox}	ΔE_{red}
1	0.9	-0.6	1.5	0.0	-0.3
1-TiO$_2$	0.9	-0.9	1.8		
2	0.9	-0.3	1.2	0.8	-0.4
2-TiO$_2$	1.7	-0.7	2.4		
3	0.9	-0.6	1.5	0.6	-0.5
3-TiO$_2$	1.5	-1.1	2.6		
4	0.9	-0.3	1.2	0.8	-0.4
4-TiO$_2$	1.7	-0.7	2.4		

It can be noticed that the reduction of all the dyes at the TiO_2 surface occurs at very similar potentials with an exception of **3-TiO$_2$** (Table 3). This materials is characterized by the lowest reduction potential amounting to -1.1 V. These values indicate high stabilization of the dye at TiO_2 surface in comparison with free dye. Upon binding all reduction potentials decrease by 0.3-0.5 V, while oxidation potentials increase by 0.6-0.8 V. Only in the case of alizarin the oxidation potential remains unaffected. This observation indicates significant stabilization of the bound dye towards both oxidation and reduction in the ground state. **2**, **3** and **4** interact with titania surface with both hydroxyl (donor) and carbonyl (acceptor) moieties, therefore both potentials are highly affected. In the case of alizarin it is a bit different, double deprotonation and interaction via chelating phenolates leaves the carbonyl moiety less involved in binding. On the other hand much stronger coupling with the surface makes direct comparison of **1** with other dyes difficult. Value of reduction potential is significantly important because reduced hybrid material has got totally different spectral character and stability leading to variant photo(electro)chemical activity. DPV curves, presented at Figure 6 concern redox potentials in the dark. Situation has change when hybrid material is exposed to light.

Photovoltage characteristic

The surface measurements was carried out for all hybrid materials deposited onto ITO slides, which do not generate any photovoltage itself. Photovoltage was registered in a real time, during irradiation of a sample by monochromatic light of variable length. Upon background subtraction the surface photovoltage spectra were obtained (Figure 7). Comparison of photovoltages of hybrid materials with the photovoltage of pure TiO_2 clearly indicates photosensitization towards visible light in the case of all studied materials, however in the case of **3-TiO$_2$** the signal is rather weak. In the case of **1-TiO$_2$**, however, the surface charge polarity is different than in the case on other materials. It is consistent with expectations. DFT modelling of excited state charge density (Figure 4) indicates positive charging of titanium center and negative charging of the exposed side of the molecule. Negative values of photovoltage are characteristic for *n*-type semiconductors, while positive value of photovoltage is characteristic for *p*-type ones. Therefore it can be concluded that the **1-TiO$_2$** material exhibits mixed photoelectrical characteristics: the inner part of particles reveals *n*-type conductivity, whereas the surface *p*-type-like behavior. This intriguing phenomenon cannot be related to adsorbate-induced band bending as this is usually negligible in the case of small particles. On the other hand adsorbate may be involved in a charge carrier trapping process. Then trapped charges generate electric field which in turn induced Dember effect opposing the diffusion-controlled phenomena within semiconductor.[53] It is consistent with the acceptor character of quinonic groups exposed at the surface in the case of alizarin.

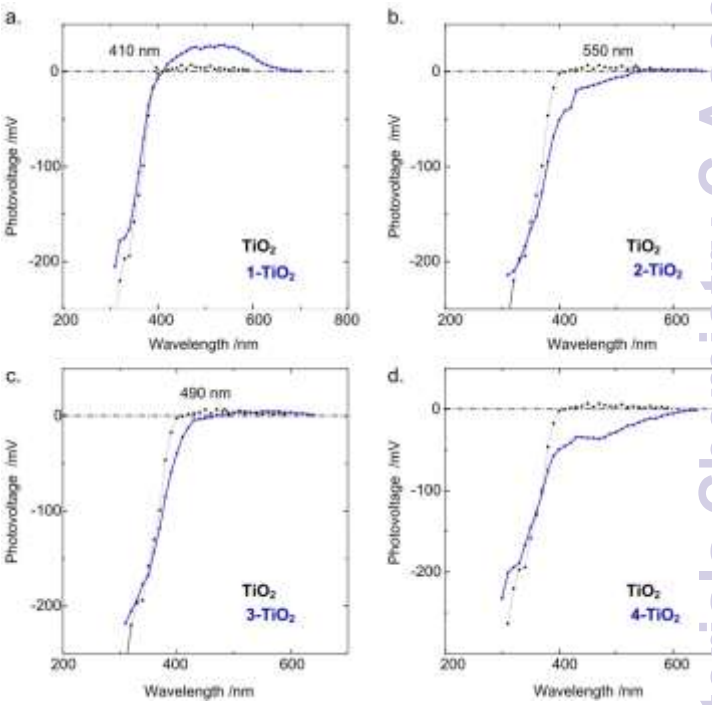

Figure 7. Surface photovoltages of different hybrid materials. Photovoltage amplitudes are presented as a function of excitation wavelength.

Photocurrent action spectra and the PEPS effect

According to Butler-Wilson equation and Schottky-Gartner model the photocurrent - potential relation is described by the following equation (3):

$$i_{ph} = \alpha W_0 q \varphi_0 \sqrt{V - V_{fb}} \qquad (3)$$

where α stands for molar absorption coefficient, W_0 is width of depletion layer at defined potential, q is electric charge, φ_0 is photon flux, V is external potential, V_{fb} is flat-band potential. This equation

assumes the linear dependence of photocurrent to square root of applied potential, when remaining parameters (α, W_0) are constant. The last condition is not always fulfilled, because W_0 in some cases depends on applied potential. Hence, there are certain deviations from presented model. All materials reveal both types of photocurrents: anodic and cathodic. Anodic photocurrent involves electrons moving into the working electrode, whereas cathodic refers to electrons transferred to the sacrificial electron acceptor present in the electrolyte (dissolved molecular oxygen). Photocurrent polarity depends on applied potential between the electrodes. In order to analyse propagation and phase transition of photoinduced electrons and holes, pulsed photocurrent spectroscopy was employed. Measured photocurrent spectra are presented as 3-D map, where photocurrent intensity is expressed as a function of applied potential and incident light wavelength (Figure 8). For all hybrid materials photocurrent in the potential range 0.8-0.2 V vs SHE can be described by equation (3). At potentials in between 0.2-0.1 V vs SHE photocurrent switching is observed. This effect also known as PEPS (photoelectrochemical photocurrent switching) effect.[1, 10, 54-56] Potentials below 0.1 V vs SHE result in photocurrents in the opposite direction (cathodic photocurrents). The switching potentials (potential at which the change of photocurrent direction occurs) of all considered materials are in the range 0.2-0.1 V vs SHE, thus slightly depends on chromophore type. However, chromophore type strongly influences cathodic photocurrent shape and intensity (Figure 8). The common feature of all hybrids is potential-controlled mechanism of photocurrent switching, thereby excitation wavelength has no impact on photocurrent direction. Anodic photocurrents are generated in hybrid materials at potentials above 0.2 V vs SHE (positive electrode polarization), whereas cathodic photocurrent occurs below 0.1 V vs SHE (negative electrode polarization). Photocurrents generated within semiconductor absorption region exhibit high amplitude, whereas photocurrent amplitudes within absorption bands of organic dyes are much lower. The latter, however, are responsible for unique photoelectrical properties of hybrid materials. Visible separation of photocurrents generated in semiconductors from photocurrents generated in molecule region suggests weak electronic coupling and photosensitization by photoinduced electron transfer (Sakata- Hashimoto-Hiramoto model).[57, 58] Photocurrent generation in the semiconductor region can be described by photoexcitation of electron from the valence to the conduction band. As a result two types of charge carriers are created: electrons in the conduction band and holes in the valence band. Electrons are able to move towards electrode (ITO) or towards electron acceptor in electrolyte, depending on the electric potential gradient. At the same time, electrons and holes can be engaged in interfacial electron transfer reactions with sacrificial reagents present in the electrolyte. The efficient holes scavenger in aqueous electrolytes is OH^-. Redox potential of $OH^{\bullet}/OH^-$ at pH of 7 is 2.31 V.[59] This potential is sufficient to reduce holes in the valence band of TiO_2, at potential of ca. 3.0 V. This indicates generation of photocurrents within TiO_2 electrode immersed in aqueous solution, without photodegradation.

At positive potentials (anodic photocurrent) the dominant photocurrent originates from TiO_2 excitation, however in the case of **1-TiO$_2$** minor photosensitization can be observed. Other materials show photosensitization only under cathodic photocurrent regime. Compounds **2**, **3**, and **4** only below 0.2 V show only minor photosensitization, whereas **1** generates photocurrent of relatively high intensity. Under negative bias potential, however, the photocurrent polarity can be changed. In this case an electron form the dye molecule is used to reduce sacrificial electron acceptor. This usually happens when the electron transfer to the conduction band (and/or to the conducting support) is thermodynamically not favoured or is slower than the reduction process. The most important factors are: energy of excitation, barrier at the interphase (Schottky barrier), electrical capacity of individual crystallites and charge distribution within photoexcited molecule. Most of these parameters depend on photoelectrode potential and incident light wavelength. Therefore changes in potential and wavelength induce photocurrent switching effects in dye-modified wide band gap semiconductors.

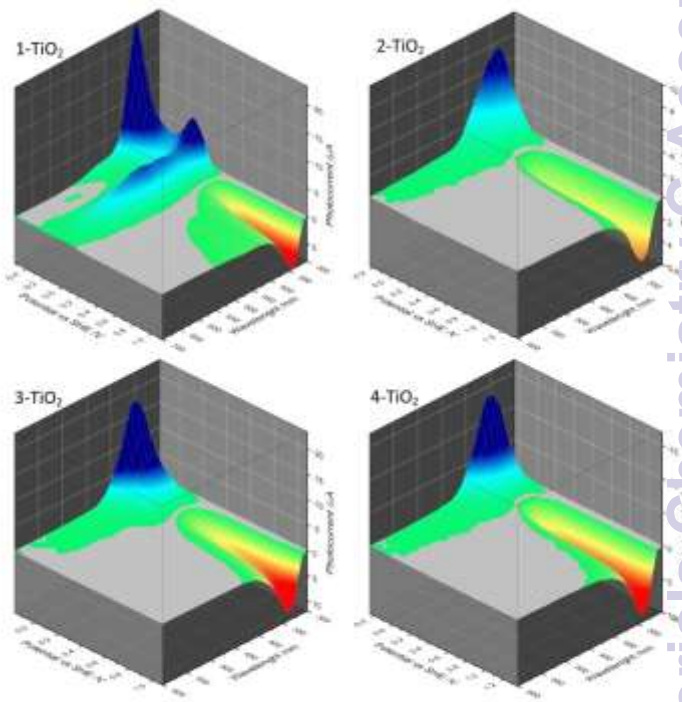

Figure 8. Photocurrent intensity of four hybrid materials as a function of wavelength of incident light and applied potential, measured in oxygenated, aqueous 0.1 M KNO_3.

Conclusions

Computational analysis indicated that dyes of very similar structure (four isomers of dihydroxyanthraquinone) have very different photoelectrochemical properties when deposited onto titanium dioxide. It is a striking phenomenon, as their properties in unbound state are much more similar. The difference is a result of different binding modes which may engage both quinonic and phenolic functionalities. Therefore the redox amphotericity of the dye is modulated by interaction with semiconducting surface. Furthermore,

interesting photocurrent switching patterns may offer a new perspective for optoelectronic logic devices, including ternary ones.

Acknowledgements

Financial support from Ministry of Science and Higher Education (grants no. UMO 2011/03/B/ST5/01495, UMO-2011/03/N/ST5/04470) and Polish Ministry of Science and Higher Education (Statutory project 11.11.180.654) is gratefully acknowledged. This research was supported in part by PL-Grid Infrastructure.

Notes and references

[a] Faculty of Non-Ferrous Metals, AGH University of Science and Technology, al. Mickiewicza 30, 30-059 Kraków, Poland.
[b] Academic Centre for Materials and Nanotechnology, AGH University of Science and Technology, al. Mickiewicza 30, 30-059 Kraków, Poland.
[*] Corresponding author: szacilow@agh.edu.pl.

1. K. Szaciłowski and W. Macyk, *Comp. Rend. Chimie*, 2006, **9**, 315-324.
2. N. R. de Tacconi, J. Carmona and K. Rajeshwar, *J. Phys. Chem. B*, 1997, **101**, 10151-10154.
3. S. Somasundaram, C. R. Chenthamarakshan, N. R. de Tacconi, Y. Ming and K. Rajeshwar, *Chem. Mater.*, 2004, **16**, 3846-3852.
4. N. R. de Tacconi, C. R. Chenthamarakshan, K. Rajeshwar and E. J. Tacconi, *J. Phys. Chem. B*, 2005, **109**, 11953-11960.
5. A. Podborska, B. Gaweł, Ł. Pietrzak, I. B. Szymańska, J. K. Jeszka, W. Łasocha and K. Szaciłowski, *J. Phys. Chem. C*, 2009, **113**, 6774-6784.
6. P. Kwolek, K. Pilarczyk, T. Tokarski, K. Lewandowska and K. Szaciłowski, *Nanoscale*, 2014, **6**, 2244-2254.
7. P. Kwolek and K. Szaciłowski, *Electrochim. Acta*, 2013, **104**, 448-453.
8. P. Kwolek, K. Pilarczyk, T. Tokarski, J. Mech, J. Irzmański and K. Szaciłowski, *Nanotechnology*, 2015, **26**, in press.
9. K. Lewandowska, A. Podborska, P. Kwolek, T.-D. Kim, K.-S. Lee and K. Szaciłowski, *Appl. Surf. Sci.*, 2014, **319**, 285-290.
10. K. Szaciłowski, W. Macyk, M. Hebda and G. Stochel, *ChemPhysChem*, 2006, **7**, 2384-2391.
11. K. Szaciłowski, W. Macyk and G. Stochel, *J. Mater. Chem.*, 2006, **16**, 4603-4611.
12. S. Gawęda, G. Stochel and K. Szaciłowski, *Chem. Asian J.*, 2007, **2**, 580-590.
13. W. Macyk, G. Stochel and K. Szaciłowski, *Chem. Eur. J.*, 2007, **13**, 5676-5687.
14. S. Gawęda, G. Stochel and K. Szaciłowski, *J. Phys. Chem. C*, 2008, **112**, 19131-19141.
15. M. Oszajca, K. L. McCall, N. Robertson and K. Szaciłowski, *J. Phys. Chem. C*, 2011, **115**, 12187-12195.
16. Y. Di Iorio, H. B. Rodríguez, E. San Román and M. A. Grela, *J. Phys. Chem. C*, 2010, **114**, 11515-11521.
17. Y. Di Iorio, R. Parra, K. Szaciłowski and M. A. Grela, *New J. Chem*, 2013, **37**, 969-976.
18. D. Chen and J. Li, *J. Phys. Chem. C*, 2010, **114**, 10478-10483.
19. M. Warzecha, M. Oszajca, K. Pilarczyk and K. Szaciłowski, *Chem. Commun.*, 2015, **51**, 3559-3561.
20. J. Kuncewicz, P. Ząbek, K. Kruczała, K. Szaciłowski and W. Macyk, *J. Phys. Chem. C*, 2012, **114**, 21762-21770.
21. M. Buchalska, M. Pacia, M. Kobielusz, M. Surówka, E. Świętek, E. Wlaźlak, K. Szaciłowski and W. Macyk, *J. Phys. Chem. C*, 2014, **118**, 24915-24924.
22. L. F. O. Furtado, A. D. P. Alexiou, L. Gonçalves, H. E. Toma and K. Araki, *Angew. Chem. Int. Ed.*, 2006, **45**, 3143-3146.
23. S. Gawęda, A. Podborska, W. Macyk and K. Szaciłowski, *Nanoscale*, 2009, **1**, 299-316.
24. R. Beránek and H. Kisch, *Angew. Chem. Int. Ed.*, 2008, **47**, 1320-1322.
25. M.-c. Long, R. Beranek, W.-m. Cai and H. Kisch, *Electrochim. Acta*, 2008, **53**, 4621–4626.
26. S. Gawęda, R. Kowalik, P. Kwolek, W. Macyk, J. Mech, M. Oszajca, A. Podborska and K. Szaciłowski, *Isr. J. Chem.*, 2011, **51**, 36-55.
27. A. Podborska, M. Oszajca, S. Gawęda and K. Szaciłowski, *IET Circ. Dev. Syst.*, 2011, **5**, 103-114.
28. K. Szaciłowski and W. Macyk, *Chimia*, 2007, **61**, 831-834.
29. W. Stier and O. V. Prezhdo, *J. Phys. Chem. B*, 2002, **106**, 8047-8054.
30. W. Stier and O. V. Prezhdo, *Isr. J. Chem.*, 2002, **42**, 213-224.
31. W. R. Duncan, W. M. Stier and O. V. Prezhdo, *J. Am. Chem .Soc.*, 2004, **127**, 7941-7951.
32. W. R. Duncan and O. V. Prezhdo, *J. Phys. Chem. B*, 2005, **109**, 365-373.
33. W. R. Duncan and O. V. Prezhdo, *J. Phys. Chem. B*, 2005, **109**, 17998-18002.
34. W. R. Duncan and O. V. Prezhdo, *Annu. Rev. Phys. Chem.*, 2007, **58**, 143-184.
35. O. V. Prezhdo, W. R. Duncan and V. V. Prezhdo, *Acc. Chem. Res.*, 2008, **41**, 339-348.
36. O. V. Prezhdo, W. R. Duncan and V. V. Prezhdo, *Progr. Surf. Sci.*, 2009, **84**, 30-68.
37. Y. Di Iorio, M. A. Brusa, A. Feldhoff and M. A. Grela, *Chem. Phys. Chem.*, 2009, **10**, 1077 – 1083.
38. R. Sánchez-de-Armas, J. Oviedo, M. Á. S. Miguel and J. F. Sanz, *J. Phys. Chem. C*, 2011, **115**, 11293–11301.
39. R. Sánchez-de-Armas, J. O. López, M. A. San-Miguel and J. F. Sanz, *J. Chem. Theory Comput.*, 2010, **6**, 2856–2865.
40. J. Mech, A. Grela and K. Szaciłowski, *Dyes Pigments*, 2014, **103**, 202-213.
41. J. F. Endicott, in *Comprehensive Coordination Chemistry II*, eds. J. A. McCleverty and T. J. Meyer, Elsevier, Amsterdam, 2003, pp. 657-730.
42. N. G. Connelly and W. E. Geiger, *Chem. Rev.*, 1996, **96**, 877-910.
43. J. Eloranta, V. Vatanen, A. Grönroos, M. Vuolle, R. Mäkelä and H. Heikkilä, *Magn. Reson. Chem.*, 1996, **34**, 898-902.
44. D. Jacquemin, J. Preat, M. Charlot, V. Wathelet, J.-M. André and E. A. Perpète, *J. Chem. Phys.*, 2004, **121**, 1736-1743.
45. W. R. Duncan, W. M. Stier and O. V. Prezhdo, *J. Am. Chem. Soc.*, 2005, **127**, 7941-7951.
46. J. Paier, M. Marsman and G. Kresse, *J. Chem. Phys.*, 2007, **127**, 024103.

47. P. Kwolek, M. Oszajca and K. Szaciłowski, *Coord. Chem . Rev.*, 2012, **256**, 1706-1731.
48. Lars Dworak, Victor V. Matylitsky and J. Wachtveitl, *ChemPhysChem*, 2009, **10**, 384 – 391.
49. J. Li, I. Kondov, H. Wang and M. Thoss, *J. Phys. Chem. C*, 2010, **114**, 18481–18493.
50. A. Nawrocka and S. Krawczyk, *J. Phys. Chem. C*, 2008, **112**, 10233–10241.
51. J. Mech, M. A. Grela and K. Szaciłowski, *Dyes and Pigments*, 2014, **103**, 202-213.
52. W. R. Duncan and O. V. Prezhdo, *J. Phys. Chem. B*, 2005, **109**, 365-373.
53. D. S. Warren, Y. Shapira, H. Kisch and A. J. McQuillan, *J. Phys. Chem. C*, 2007, **111**, 14286-14289.
54. M. Hebda, G. Stochel, K. Szaciłowski and W. Macyk, *J. Phys. Chem. B*, 2006, **110**, 15275-15283.
55. K. Szaciłowski and W. Macyk, *Solid State Electron.*, 2006, **50**, 1649-1655.
56. K. Szaciłowski, W. Macyk and G. Stochel, *J. Mater. Chem.*, 2006, **16**, 4603–4611.
57. T. Sakata, K. Hashimoto and M. Hiramoto, *J. Phys. Chem.*, 1990, **94**, 3040-3045.
58. O. Kitao, *J. Phys. Chem. C*, 2007, **111**, 15889-15902.
59. A. G. Sykes, *Advances in Inorganic Chemistry*, Elsevier Science, 1989.

Table of contents figure & text

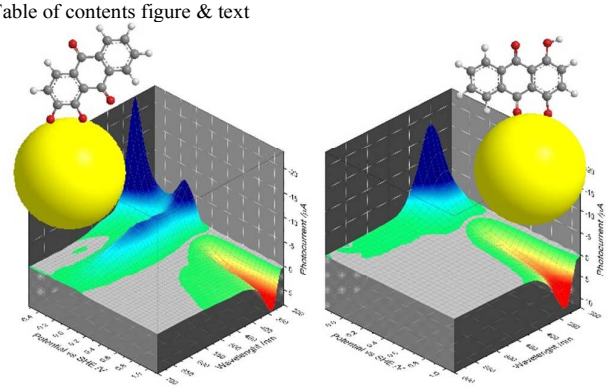

Quantum-chemical modelling of dihydrixyanthraquinone complexes of titanium (IV) reflects photochemistry of titanium dioxide photosensitized with anthraquinone dyes.